Letters in Applied NanoBioScience
Open-Access Journal (ISSN: 2284-6808)

Review
Volume 14, Issue 1, 2025, 35
https://doi.org/10.33263/LIANBS141.035

Suitability of Reduced Graphene Oxide(rGO) Nanocomposites for Enhanced Water Splitting: A Review

Salman Ahmad Fani [1], Subhojyoti Sinha [2], Aayush Gupta [3] Shahid Ahmad Shah [1] Deepak Basandrai [1,*]

[1] Department of Physics, Lovely Professional University, Punjab-144411, India
[2] Department of Physics and Nanotechnology, SRM Institute of Science and Technology, Kattankulathur, Tamil Nadu-603203, India
[3] Functional Materials Lab, Department of Mechanical Engineering, GLA University, Mathura, Uttar Pradesh-281406, Indiax
* Correspondence: deepakbasandrai@gmail.com; (D.B.);

Scopus Author ID 57191920826
Received: 7.07.2023; Accepted: 23.11.2023; Published: 28.09.2024

Abstract: Green energy resources as a replacement for fossil fuels have become a topic of concern amongst researchers. The creation of energy using water splitting is emerging as a very permissive source in this context that can generate H_2, which can be considered a next-generation fuel. Even though there is considerable research in this field, the efficiency of H2 production (HER; hydrogen evolution reaction) is still not up to the mark. Different catalysts in combination with nanostructured metal oxides, metal phosphide, 2D materials, graphene, and its derivatives have been showing promising results in improving process efficiency. The present review work offers a comprehensive study of numerous methods of water splitting and examines several nanocomposites based on reduced graphene oxide (rGO). The electrochemical properties of rGO-based nanocomposites, including current density, overpotential, and Tafel slope, are analyzed and compared herein. In addition, the paper reviews ZnO/rGO nanocomposites in various forms and analyzes their photochemical and photoelectrochemical properties for water splitting. Furthermore, this review analyzes the photoelectrochemical performance of ZnO/rGO heterostructures with Cu_2O, CeO_2, and metals such as Ni, Co, and Mn. It provides insights into the advancements and potential of rGO-based nanocomposites for efficient Water splitting and can serve as a roadmap for future research in this field.

Keywords: green energy resources; water splitting; electrochemical properties; photochemical; photoelectrochemical.

1. Introduction

Recently, there has been continuous research in the field of water splitting (WS) for eco-friendly (green) H_2 generation by the reaction $2H_2O \rightarrow 2H_2 + O_2$ which is referred to as a 'water splitting' reaction. It can be done by conventional WS process (as shown in Figure 1) with hydrocarbons or coal as a primary energy source, electrochemical/photochemical/photoelectrochemical water splitting, photobiological methods, or thermochemical cycle process [1].

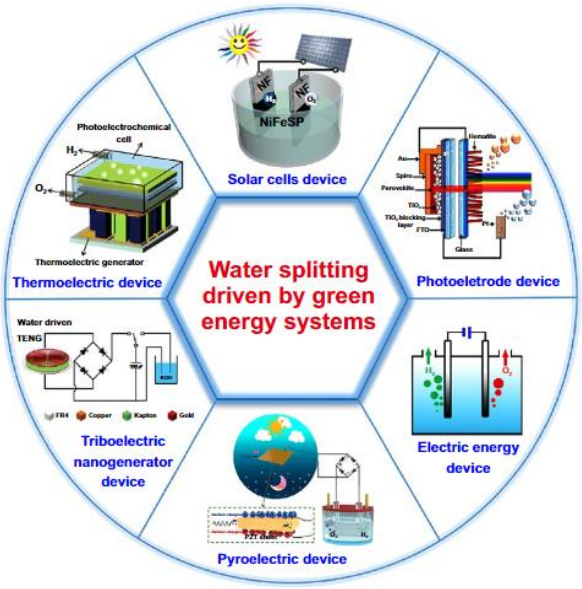

Figure 1. WS determined by diverse green energy systems [2].

Electrochemical WS is an effective, cheap, and promising technology. This gaseous H_2 can be used directly or stored as chemical energy as an M-H bond in metal hydrides, which would be used as futuristic sustainable energy [3]. However, the challenge associated with water splitting is grid scalability. Worldwide research groups are working on different parameters of the WS process to overcome this bottleneck and change the current fossil fuel-based energy scenario. But at the same time, industrial H_2 production during natural gas refining produces a large amount of CO_2 emission, which is undesirable. So, only renewable resources should be recommended to produce 'Green H_2'. Renewable energy resources include (i) sunlight, (ii) wind energy, and (iii) tidal energy. For the effective use of sunlight, the construction of photoelectrodes to absorb sunlight efficiently is followed by the generation of potential difference (i.e., photovoltage) [2]. This can be supplied as the external energy for electrocatalysis. Solar cells are another possible approach to supplying energy for this process. Thermoelectric materials can also convert the heat produced by sunlight into electrical energy and serve as a clean external energy source [4]. Wind and tidal energy can also be used for HER with the help of triboelectric nanogenerators [5-7].

H_2 has emerged as a promising energy source due to its high energy density and minimal environmental impact, but production efficiency through HER still needs improvement [8]. Researchers have recently explored various catalysts combined with nanostructured metal oxides [9], metal phosphides, 2D materials, graphene, and their derivatives to enhance HER efficiency. Among these catalysts, functional nanomaterials like multiferroics [10,11] and metal phosphides decorated with rGO and ZnO/rGO have shown significant potential for efficient WS. In this review paper, we will focus on these catalysts' electrochemical and photoelectrochemical properties and compare their effectiveness in parameters like current density, overpotential, stability, and Tafel slope.

1.1. Electrochemical water splitting.

Electrochemical WS is a viable technique for producing clean H_2 fuel from renewable energy sources. In this process, water is oxidized at the anode, and protons are reduced at the cathode, forming H_2 gas. For this technique to be used in practice, effective and reliable electrocatalysts for total WS are essential. To have better control and accuracy of the

electrochemical reactions, a 3-electrode setup is frequently employed in electrochemical water splitting. In this configuration, a reference electrode is attached to the anode (working electrode) and cathode (counter electrode) to measure the electrode potential and steady voltage across the cell. The reference electrode is made of an inert metal, such as Ag/AgCl, and its potential is well-defined [12]. It is possible to compare and improve the performance of various electrocatalysts by adjusting the voltage, current density, and electrolyte composition. The reference electrode can also be used as a diagnostic tool to find any alterations in electrode potential and spot any potential degradation or fouling of the electrode surface [13,14]. This review paper thoroughly summarizes current developments in electrochemical water splitting, covering core concepts, significant difficulties, and potential approaches for boosting the effectiveness and longevity of electrocatalysts based on rGO and rGO/ZnO heterostructures.

1.2. Photochemical water splitting.

Another potential method that uses solar energy to produce H_2 gas from water is photochemical water splitting, as shown in Figure 2.

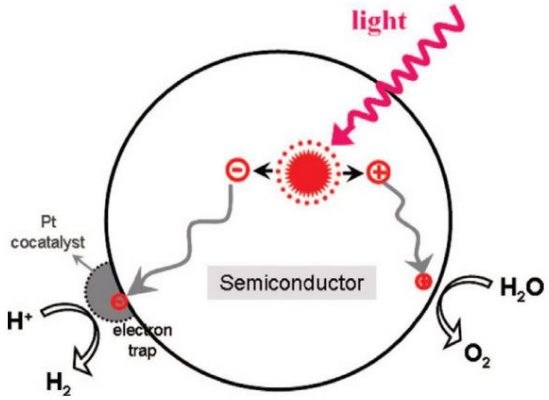

Figure 2. Transfer of charges between host and co-catalysts in photochemical water splitting [15].

In this process, the catalyst absorbs light coming from any natural or artificial source and produces exciton ($e^- - h^+$) pairs, which initiates the water-splitting reaction. The process uses a reaction vessel with a photocatalyst coated on substrates like Fluorine-doped Tin Oxide, an electrolyte, and a light source like the sun or any artificial light source like Xe flashlight. A few essential components must be assembled for a photochemical water-splitting system using a nanocomposite photocatalyst. The first part is the photocatalyst material, which consists of a semiconductor material, like TiO_2 or CdS, combined with a small quantity of a co-catalyst material, like Pt or Pd [16,17]. The substrate on which the nanocomposite photocatalyst is placed is the second element of the system. This can be a glass or metal substrate such as FTO glass, and the nanocomposite photocatalyst is placed as a thin film or nanoparticulate layer on top of it. A sacrificial reagent, such as a hole scavenger or electron donor, such as methanol or Na_2SO_3, is added to the solution for an efficient water-splitting reaction. The fourth component of the system is the light source, which is utilized to stimulate the photocatalyst and enterprise to initiate the water-splitting reaction. It could be actual sunlight or an artificial light source like a powerful LED or a solar simulator. The system's performance can be evaluated by measuring the amount of gaseous H_2 produced over time and, hence, the efficiency of the process in terms of quantum yield or solar-to-hydrogen value [1]. The optimization of photocatalyst, electrolyte solution, and light source can be used as a probe to maximize the efficiency of photochemical reaction [18,19].

1.3. Photoelectrochemical water splitting.

PEC water splitting, shown in Figure 3, is another potential method for sustainable and clean energy production by using semiconducting material as photoanode to harvest solar energy and produce gaseous H_2 by decomposing water molecules due to both high efficiency and inexpensive [21]. In PEC water splitting, the three-electrode setup is typically used. A working electrode (photoelectrode), a counter electrode, and a reference electrode are all components of this system. The working electrode usually comprises a semiconductor nanomaterial that absorbs light and produces exciton. The electrode material is usually placed on a glass or FTO because of its good conductivity, transparency, and stability in an alkaline electrolyte medium [22]. The electrons produced at the working electrode are gathered by utilizing a counter electrode. Then the electrons are transmitted to the electrolyte, where they can react with water molecules to produce gaseous H_2. The counter electrode is often made of a conductive material, such as Pt or IrO_2. The reference electrode is utilized to monitor the reaction''s progress and the ideal potential of the working electrode operating for water splitting;'s progress and the ideal potential of the working electrode operating for water splitting. The three-electrode system ensures that the reaction continues successfully without producing any undesirable adverse reaction products and enables precise control over the potential at the working electrode.

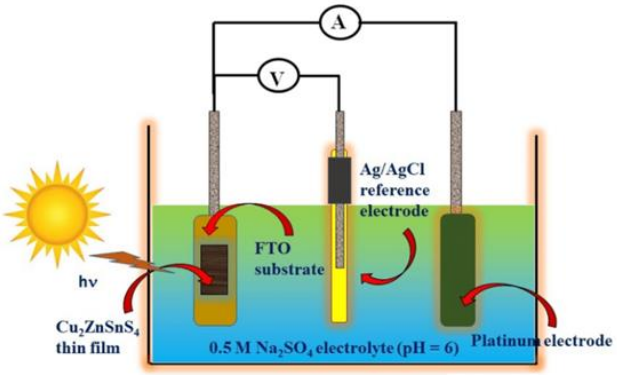

Figure 3. Three-electrode system for photoelectrochemical setup [20].

One important aspect that affects the PEC 'cell's overall performance is the 'photoelectrode's efficiency, i.e., current density (CD), which represents the extent of electrical energy available to power the reaction. Efficiency rises along with CD up to a certain point, and beyond that limit, it can cause catalyst instability in terms of increased recombination and thermal degradation. To achieve the required balance between efficiency and stability, it is crucial to optimize the photoelectrode's CD density by adjusting the electrode material's features, such as its defects, bandgap, and morphology [17]. High current densities and efficiencies can be attained through careful optimization, producing robust and effective PEC cells for industrial water-splitting applications. In this review work, we have reviewed several ZnO/rGO heterostructures as photoelectrodes for efficient PEC water splitting [16,23].

2. Results and Discussion

2.1. Review the rGO-based nanocomposite for electrochemical water splitting.

Wang *et al*. (2016**)** synthesized CoP_2/rGO using a low-temperature phosphidation reaction for both HER and OER (oxygen evolution reaction) with ultrahigh catalytic activity.

For HER, an overpotential of 88mV and 106mV to drive 10mA/cm^2 and 20mA/cm^2 of CD showed better results than monolithic CoP_2. The obtained Tafel slope was also lower for CoP_2/rGO nanocomposite, which was less than bulk CoP_2 and even better than commercial Pt/C catalysts. In addition, CoP_2/rGO exhibited an onset overpotential of 38mV for HER (0.5M H_2SO_4), which was smaller than bulk CoP_2. For OER, 10mA/cm^2 and 20mA/cm^2 at 300mV and 330mV as overpotentials were obtained for CoP_2/rGO, which was slightly larger than RuO_2. Interestingly, beyond 360mV (overpotential), the current density of CoP_2/rGO surpasses RuO_2 with 96mV/dec as the Tafel slope. Furthermore, under strong alkaline conditions, CoP_2/rGO exhibited superior stability, which was better than CoP_2 [24].

Romeiro *et al*. (2017) synthesized rGO-ZnO nanocomposite (8rGO-ZnO and 16rGO-ZnO, according to weight taken in synthesis) by a microwave-hydrothermal method [25-27]. The authors further studied the electrochemical characteristics of nanocomposite films by cyclic voltammetry and chronoamperometry analysis. The 16rGO-ZnO nanocomposite exhibited impressive results of 0.48V as onset potential at pH = 7.0 and 0.67V as onset potential at pH = 13 for OER. It also showed the highest current density during electrolysis amongst ZnO and 8rGO-ZnO stable current density as a function of time [28].

Narwade *et al*. (2019) used a chemical synthesis method to prepare Ni/NiO on rGO (Ni/NiO@rGO), a bifunctional electrocatalyst. Glassy carbon (GC) modified with Ni/NiO@rGO, Pt foil, and saturated calomel electrode (working electrode), counter electrode, and reference electrode have been taken, respectively. Ni/NiO@rGO demonstrated an onset potential of -0.4mV vs RHE and 582mV overpotential at 10mA/cm^2 in HER while exhibited 480mV overpotential at 10mA/cm^2 with an onset potential of 1.6V vs. RHE under OER. In addition, Tafel slope values of 63mV/dec and 41mV/dec were obtained for HER and OER, respectively [29].

Maghrabi *et al*. (2020) fabricated Ni/NiO-TiO_2/rGO on porous carbon cloth using the PECVD process proposed by Nada *et al*. [30,31]. The electrochemical assessments were achieved using a three-electrode configuration using carbon cloth, Ag/AgCl, and graphite as working, reference, and counter electrodes (respectively) in 0.5M H_2SO_4 electrolyte solution. During HER, Ni/NiO-TiO_2/rGO@CC exhibited 0.13V overpotential @ 10mA/cm² and an onset potential of 30mV during OER. A Tafel slope of 40mv/dec was also obtained during HER. Also, Ni/NiO-TiO_2/rGO showed long-term durability with high activity up to 60h in 0.5M H_2SO_4 medium [32].

Zhi-yi Pan *et al*. (2020) synthesized $CoNiO_2$@rGO on Ni- foam by hydrothermal method. The authors did the electrochemical tests on a standard three-electrode system. The reversible hydrogen electrode is a reference electrode, the carbon rod electrode is a counter electrode, and the $CoNiO_2$@rGO/NF is the working electrode. According to the authors, $CoNiO_2$@rGO/NF had a low onset potential of 1.48V compared to RHE. For OER, they reported a 272mV overpotential to obtain a current density of 100mA/cm^2, and for HER, a 126mV overpotential to obtain a current density of 10mA/cm^2.The Tafel slope value for OER was 49mV/ dec, and for HER it was 72mV/dec. The authors also reported a current density of 10mA/cm² @ an overall overpotential of 1.56V. This nanosheet array maintained stability for at least 40h [33].

Cao *et al*. (2021) Synthesized $NiFe_2O_4$@N/rGO bifunctional electrocatalysts using PVP self-template method. The authors studied the electrochemical characteristics of these electrocatalysts in a standard three-electrode system, taking graphite rod and platinum wire as counter electrodes for HER and OER, respectively Ag/AgCl as reference electrode, and for the

working electrode, catalyst-modified Ni foams are used. The authors reported that catalytic activity for OER showed an overpotential of 252mV, 287mV, 276mV, and 283mV for $NiFe_2O_4$@N/rGO-800, $NiFe_2O_4$@N/rGO-700, $NiFe_2O_4$@N/rGO-900, and $NiFe_2O_4$@rGO-800 respectively to achieve a current density of 20mA/cm². They also reported when current density reached up to 100mA/cm², the overpotentials reached 290mV, 332mV, 321mV, and 318mV for $NiFe_2O_4$@N/rGO-800, $NiFe_2O_4$@N/rGO-700, $NiFe_2O_4$@N/rGO-900, and $NiFe_2O_4$@rGO-800 respectively. For analyzing the kinetics of OER Tafel slope values were calculated by the authors to be 49.7mV/dec, 73.6mV/dec, 59.5mV/dec, and 52.4mV/dec for the $NiFe_2O_4$@N/rGO-800, $NiFe_2O_4$@N/rGO-700, $NiFe_2O_4$@N/rGO-900 and $NiFe_2O_4$@rGO-800 samples respectively. The authors reported the catalytic activity for HER showed an overpotential of 157mV, 169mV, 167mV, and 186mV for $NiFe_2O_4$@N/rGO-800, $NiFe_2O_4$@N/rGO-700, $NiFe_2O_4$@N/rGO-900, and $NiFe_2O_4$@rGO-800 respectively to obtain a current density of 10mA/cm². They also reported that when current density reached upto 100mA/cm², the overpotentials reached 271mV, 331mV, 305mV, and 335mV for $NiFe_2O_4$@N/rGO-800, $NiFe_2O_4$@N/rGO-700, $NiFe_2O_4$@N/rGO-900 and $NiFe_2O_4$@rGO-800 respectively. While analyzing the kinetics of HER, Tafel slope values obtained by the authors for $NiFe_2O_4$@N/rGO-800, $NiFe_2O_4$@N/rGO-700, $NiFe_2O_4$@N/rGO-900, and $NiFe_2O_4$@rGO-800 were 94.7mV/dec, 121.2mV/dec, 123.5mV/dec and 129.9mV/dec respectively. $NiFe_2O_4$@N/rGO-800 showed the lowest overpotential for HER and OER. For overall water splitting, the authors used $NiFe_2O_4$@N/rGO-800 as both cathode and anode in a two-electrode electrolytic cell. The authors reported $NiFe_2O_4$@N/rGO-800 reached a current density of 10mA/cm² and 20mA/cm² @ overpotentials of 1.6V and 1.67V, respectively, and good stability of 24h achieved at 10mA/cm² and 20mA/cm² [34].

Arif *et al*. (2021) synthesized NiVB/rGO (nickel vanadium boride/rGO) nanocomposite by chemical reduction method. For electrochemical studies of NiVB/rGO, the authors used a standard three-electrode system in which NiVB/rGO modified glassy carbon electrode (GCE) is used as working, Ag/AgCl is used as a counter electrode, and Pt wire as a reference electrode. The authors reported that At OER NiVB/rGO, an overpotential of 0.267V was required to achieve a current density of 10 mA/cm². They also reported a 44mV/dec Tafel slope value for OER, and at HER, they reported an overpotential of 0.151V to achieve a current density of 10mA/cm² and a Tafel slope value of 88mV/dec. For the overall water splitting measurement, the authors used both cathode and anode electrodes made with NiVB/rGO in a two-electrode system in which the electrodes act for HER and OER. To attain current densities of 10mA/cm^2 and 100mA/cm^2, the authors reported overall overpotentials of 1.56V and 1.76V, respectively. There was a negligible fluctuation in current density, showing good stability of NiVB/rGO nanocomposite [35].

Li *et al*. (2022) synthesized $NiCo_2S_4$/N, S co-doped rGO (NCS/NS-rGO) by one-pot hydrothermal method. The authors performed electrochemical characterization using a standard three-electrode system in which the working electrode was fabricated using NCS/NS-rGO loaded Ni foam (1cm x 1cm), reference electrode by Ag/AgCl, and counter electrode by pt foil. To reach the current density of 10mA/cm², the authors reported the overpotential of 92.7mV for NCS/NS-rGO at HER. For HER they reported a Tafel slope value of 77.6mV/dec. To achieve a current density of 10mA/cm² at OER. The authors reported an overpotential of 253.4 mV. A Tafel slope value of 71.7mV/dec at OER was also reported. For overall water splitting measurement, the authors used cathode and anode electrodes made with NCS/NS-rGO in a two-electrode system where the electrodes act for HER and OER. The authors achieved an

onset potential of 1.58V and an overpotential of 348mV at 10mA/cm². Also, the authors reported that NCS/NS-rGO showed a stable current density of around 10mA/cm² after 10h of overall water splitting; stability was up to 93% [36].

Kareem *et al*. (2022) have synthesized Ni_2P-N, S-rGO (Ni_2P nanoparticles supported on nitrogen, sulfur-reduced graphene Oxide) by hydrothermal method and reported promising HER. The authors also synthesized Ni_2P-rGO, Ni_2P-MWCNT, and Ni_2P-C by the same method concerning rGO, MWCNT (Multi-walled carbon nanotubes), and Vulkan Carbon as N, S-rGO used to synthesize Ni_2P-N, S-rGO. Further, the authors analyze the obtained electrocatalysts. For electrochemical characterization, the authors used PINE RDE (Rotating disk electrode) as a working electrode, a 10mm diameter acid-treated graphite rod as a counter electrode, and commercial Ag/AgCl as a reference electrode. The authors analyzed the overpotential to be 179mV, 269mV, 331mV, 368mV, and 552mV for electrocatalysts Ni_2P-N, S-rGO, Ni_2P-rGO, Ni_2P-MWCNT, Ni_2P-C, and pure Ni_2P respectively at 10mA/cm² current density. The Tofel slope values of synthesized electrocatalysts were calculated as 71, 90.8, 139.4, 169, and 181.5mV/decade for Ni_2P-N, S-rGO, Ni_2P-rGO, Ni_2P-MWCNT, Ni_2P-C, and pure Ni_2P, respectively. Ni_2P-N and S-rGO showed the highest catalytic activity towards HER amongst other synthesized electrocatalysts. Ni_2P-N, S-rGO showed the lowest overpotential of 179mV at 10mA/cm² current density and Tofel slope value 71mV/decade [37].

Table 1. Abstract the electrochemical activities towards HER and OER of rGO-based nanocomposite electrocatalysts for overall water splitting.

Sr. No.	Catalyst	Synthesis Method	Current Densities (mA/cm²)		Tafel Slope (mV/dec.)		Overpotential (mV)		Ref.
			HER	OER	HER	OER	HER	OER	
1	CoP_2/rGO	low-temperature phosphidation	10 20	10 20	50	96	88 106	300 330	[24]
2	16rGO-ZnO	Microwave Hydrothermal	-	-	-	-	480 onset	-	[28]
3	Ni/NiO@rGO	Chemical Synthesis	10	-	63	41	582	480	[29]
4	Ni/NiO-TiO_2/rGO@CC	PECVD	10	-	40	-	130	30 onset	[32]
5	Ni/NiO-rGO@CC	PECVD	10	-	54	-	244	90 onset	[32]
6	$CoNiO_2$@rGO/NF	Hydrothermal	10	100	72	49	126	272	[33]
7	$NiFe_2O_4$@N/rGO-800	PVP self-template	10	20	94.7	49.7	157	252	[34]
8	NiVB/rGO	Chemical reduction	10	-	88	44	151	267	[35]
9	NCS/NS-rGO	one-pot hydrothermal	10	-	77.6	71.7	92.7	253.4	[36]
10	Ni_2P-N, S-rGO	Hydrothermal	10	-	71	-	179	-	[37]
11	Ni_2P-rGO	Hydrothermal	10	-	90.8	-	269	-	[37]

2.2. Review on ZnO/rGO-based heterostructure for photochemical and photoelectrochemical water splitting.

Yusoff *et al*. (2015) investigated the photoelectrochemical activity of core-shell Fe_3O_4-ZnO nanoparticles on reduced graphene oxide sheets (rGO) hetero-nanostructure for water splitting. The authors synthesized the samples through hydrothermal synthesis with different weight ratios of Fe_3O_4-ZnO and rGO. Then, the authors performed a photoelectrochemical analysis using a conventional three-electrode system with a screen-printed electrode (SPE) modified with the Fe_3O_4-ZnO/rGO nanocomposite. The authors used linear sweep voltammetry (LSV) to analyze the photoelectrochemical activity of the samples under the

irradiation of simulated solar AM 1.5G in the presence of 0.1M KOH. According to the authors, upon irradiation, the Fe_3O_4-ZnO/rGO nanocomposites showed a sign of an n-type semiconductor, resulting from an increase in anodic current from 0.6V to 1.33V vs. RHE. The authors also reported the greatest photocurrent density of 850µA/cm^2 at 1.23V vs. RHE was achieved by the Fe_3O_4-ZnO/rGO (1:1:4) nanocomposite; also, the photocurrent density of bare ZnO was the lowest. The photoelectrochemical responses reported by the authors of the various modified electrodes arranged from highest to lowest Fe_3O_4-ZnO/rGO (1:1:4) > Fe_3O_4-ZnO/rGO (1:1:30) > Fe_3O_4-ZnO/rGO (1:1:2) > ZnO/rGO > Fe_3O_4/rGO > Fe_3O_4-ZnO > Fe_3O_4 > ZnO. Due to the huge electrode-electrolyte interfacial contact area and the robust intimate interaction between the ternary Fe_3O_4-ZnO and rGO, Fe_3O_4-ZnO/rGO nanocomposite demonstrated the greatest photocurrent across all compositions. The authors discussed that the electrical interaction and interfacial electron transport at the electrode/electrolyte interface were the two aspects of improved PEC water-splitting. This improved photoelectrochemical water-splitting efficiency was further supported by the poor rate of recombination of electron-hole pairs in the Fe_3O_4-ZnO/rGO (1:1:4) nanocomposite, which was shown by photoluminescence study [38].

Bai *et al*. (2015) described the $ZnIn_2S_4$/RGO/ZnO nanocomposites' performance as photocatalysts for water splitting. The authors synthesized ZnO NAs on FTO using a hydrothermal method and synthesized $ZnIn_2S_4$/RGO using a solvothermal method. They used ZnO NAs as a substrate for depositing the $ZnIn_2S_4$/RGO nanocomposite via dip-coating. The authors used an electrochemical workstation with AM1.5 G illumination to perform the PEC characterizations. They reported that adding rGO increased the photoanode's surface areas and accelerated the water oxidation process at ZnO/electrolyte interfaces. The authors also reported that ZnO NAs/rGO achieved a photocurrent density of 1.43mA/cm^2, higher than that of pure ZnO NAs.

Furthermore, the authors also reported that the highest photocurrent density of 2.25mA/cm^2, was achieved by adding $ZnIn_2S_4$ to the ZnO NAs/RGO nanocomposite. This photocurrent density was 1.6 and 2 times greater than that of ZnO NAs and ZnO NAs. The authors discussed that the enhanced photocatalytic activity of the $ZnIn_2S_4$/RGO nanocomposites could be attributed to the synergistic effect between the RGO and $ZnIn_2S_4$, which improves the transport of electrons and reduces the electron-hole recombination rate [39].

Khan *et al*. (2017) synthesized ZnO/rGO nanowire arrays (NWAs) on FTO using the sonication-assisted hydrothermal method. The authors reported that the electrolyte used for the photoelectrochemical water splitting test was done using 0.5M sodium sulfate (Na_2SO_4) in distilled water. To measure photocurrent, the authors used a typical 3-electrode system with a reference electrode made of Ag/AgCl, the counter electrode made of platinum foil, and rGO/ZnO NWAs as the working electrode was utilized. The photo-potential electrodes and current are controlled by a potentiostat (Autolab). A xenon lamp was used to simulate a light with a power density of 100 mW/cm^2. The visible component of the light spectrum was utilized after the filtration of UV spectrum part using a UV cut-off filter. The voltage sweep range was maintained between -1 and 1 volts. The authors reported that in the absence of sunlight, no appreciable photocurrent was noticed for the material. This finding suggested to the authors that materials become inactive in the dark. Yet, even in the dark, the minimal current density is seen due to overpotential at high voltage. The authors additionally reported that under the illumination of solar simulators, the maximum value of photocurrent is reached to 2.4mA/cm^2

at 0.8V. The oxygen evolution reaction (OER) was fairly dominant for the material at the specified voltage range, as evidenced by the LSV measurements of positive photocurrent density under solar visible light luminescence [40].

Ghorbani *et al*. (2018) synthesized porous ZnO/rGO nanocomposite using the sol-gel method. As-prepared sols with various concentrations of GO were utilized. The thin films were coated on fluorinated tin oxide (FTO) glasses. The authors used an Autolab model 273A potentiostat/galvanostat to conduct electrochemical tests. A standard three-electrode photoelectrochemical cell was used, with the working electrodes being ZnO or ZnO/rGO, the counter electrode being a platinum wire, and the reference electrode being Ag/AgCl. An aqueous Na_2SO_4 solution (0.5mol/L) was employed as the electrolyte. A UV lamp-equipped optical bench held the photoelectrochemical cell. The applied external potential was altered from 0 V to +1.5V in relation to Ag/AgCl. The authors reported that the electrodes exhibit very little capacitive current in the darkness, and the OER is indicated by the current at potentials greater than 1.34V. The increase in current density with increasing anodic bias under the illumination condition is evidence of the n-type nature of the pure ZnO and the ZnO/rGO nanocomposite samples. They also reported that the performance of electrodes in photoelectrochemical reactions is enhanced by adding rGO to the ZnO matrix. This was largely due to the efficient e-collection and transit properties of rGO, which greatly inhibit the recombination of photogenerated e- - h+ pairs.

Additionally, the authors described that the ZnO 'nanostructures' spherical shape and hierarchical porosity promote effective interactions between H_2O molecules and ZnO surface atoms. The authors reported that owing to an increment in no. of photogenerated charge carriers, the nanocomposite containing 1mg/mL rGO exhibits the greatest photocurrent density of 1.02mA/cm^2 at 1.5V vs. Ag/AgCl. The photocurrent density decreases when the rGO concentration rises from 1mg/mL to 2mg/mL. This may result from the clumping of rGO sheets and the lower absorbance at higher rGO concentrations [41].

Zhang *et al*. (2018) first synthesized ZnO/rGO nanocomposite on FTO glass, and then the authors used a modified photochemical method to synthesize M-Bi/rGO/ZnO (M= Ni, Co, Mn). Then, the authors did photoelectrochemical tests in a 3-electrode system (electrode as Pt plate, FTO substrate deposited with M-Bi/rGO/ZnO as working photoelectrode, and the reference electrode was made of Ag/AgCl). The author did LSV with a voltage that was swept at a rate of 10mV/s while exposed to simulated solar light with an AM 1.5G spectrum and a light intensity of 100mW/cm^2 (equal to 1 sun). The author reported that the performance was best in the Ni-Bi/rGO/ZnO sample. At 1.23V, the water oxidation photocurrent increased by 0.86mA/cm2 and there was a cathodic shift of the onset potential of 0.17V (from 0.58 to 0.41V) compared to ZnO. The Co-Bi/rGO/ZnO sample, in contrast, at 1.23V, had a photocurrent density of 0.80mA/cm^2 and a cathodic shift of 0.12V in the onset potential. As reported by the authors, with only a 0.04 V shift in the onset potential and a photocurrent density of 0.69mA/cm^2, the Mn-Bi/rGO/ZnO sample was less active. The authors also reported that to assess the 'photoanodes' stability at 1.23V the potentiostatic measurements were made. 'ZnO's photocurrent density rapidly decreased upon exposure to light, falling to 0.22mA/cm^2 (a 37% decrease), but the M-Bi/rGO/ZnO composites displayed superior stability, seeing a decrease of less than 9% [42].

Wang *et al*. (2020) cast off a one-step microwave-abetted solvothermal method to create ZnO hollow spheres on rGO nanosheet. The authors reported that the resulting product, ZrG-1, had a 1% GO content in comparison to the mass of ZnO. The authors synthesized further

samples ZrG-2, ZrG-0.5, ZrG-0.2, and ZnO by varying mass ratios of GO to ZnO (2, 0.5, 0.2, and 0 percent), respectively. The authors reported that hydrogen was evolved by photocatalysis in a sealed glass system. Normally, 0.5g of the sample is dissolved in 0.1L of distilled water with the sacrificial reagents Na_2SO_3 (0.25mol/L) and Na_2S (0.35mol/L). 30 minutes of N_2 deaeration of the suspension were followed by 300 watts of Xenon illumination. The authors used a gas chromatograph (SP-7820, TCD) to find the gases that were generated. The authors reported HER was lowest in the ZnO sample, which has a value of 279.4µmol/h/g.

The high rate of photoinduced e- and h+ pair recombination may explain this. Unexpectedly, the ZrG-0.2 nanocomposite demonstrates a significantly improved HER of 427.1µmol/h/g. This is due to 'rGO's ability to serve as an electron receiver with a 2D nanosheet structure, which is advantageous for the movement of electrons in photocatalytic systems. They also reported that for the ZrG-1 nanocomposite, hydrogen evolution occurs at 648.1µmol/h/g, the highest rate of HER among the synthesized nanocomposites. The authors discussed the following three factors that can be used to explain the good HER of ZrG-1. First, during the photocatalytic reaction, the ZrG-1 nanocomposite showed a greater number of photoexcited charge carriers;; higher surface-active areas may be the cause. Second, the ZrG-1 sample shows the slowest recombination rate for photoinduced e- h+ pairs, which is the cause of the lowest photoluminescence emission intensity. Finally, and probably most crucially, the synthesis-produced extraordinary interface between ZnO and rGO strongly encourages the separation and transfer of the interfacial carriers in a spatially accessible manner. As reported by the authors, the HER of ZrG-2 shows a little decline from 648.1 to 518.8µmol/h/g with a GO increment of 1 to 2 percent by mass. The drop in photocatalytic performance that has been seen may be explained by the following facts: When rGO concentration reaches a certain level (1%), rGO and ZnO may compete to absorb light, which might deactivate HER by blocking some UV light from reaching 'ZnO's surface. On the other hand, excessive rGO could function more like a recombination hub than an electron pathway [43].

Murali *et al*. (2020) synthesized ZnO-CeO_2-rGO via the hydrothermal method by varying weight proportions of CeO_2 and ZnO and evaluated its potential in photoelectrochemical water splitting. Photoelectrochemical measurements were carried out by the authors in a three-electrode design using a Gamry 600 D electrochemical workstation, and for electrolyte, Na_2SO_4 solution was used. Linear sweep voltammetry (LSV) scans were conducted by the authors under light illumination using a xenon flashlight and in the dark. The authors reported that the ZCG3 electrode (85:15 mass proportion of ZnO and CeO2, respectively) displayed the least photocurrent onset potential at −0.45V vs. Ag/AgCl and produced a good photocurrent density of 0.69mA/cm^2 at 1.5V due to its excellent charge transfer and separation. These findings by Murali *et al*. suggest that the ZnO-CeO_2-rGO ternary nanocomposite has the potential to be used in PEC water-splitting applications, with performance dependent on both the photocurrent density and onset potential [44].

Shanmugasundaram *et al*. (2021) utilized a simple two-step RF sputtering-annealing growth method to fabricate FTO/Cu_2O (FC)-based photocathodes, as well as FTO/Cu_2O/ZnO (FCZ) and FTO/Cu_2O/ZnO/rGO (FCZG)-based photoanodes. The authors performed the PEC test in a standard three-electrode system. For illumination AM 1.5G with a power density of 100mW/cm^2 was used. The authors reported that the bare Cu_2O photoelectrode current density based on (Cu_2O was sputtered on FTO with various thicknesses) FC3 > FC2 > FC1 were ~ 3.27, 2.64, and 1.53mA/cm^2, respectively, at 0V vs. RHE. The authors discussed that the grain size and increased surface roughness of the photoelectrode produced at a higher sputtering

duration may be used to explain the increase in current density. The current density increased with increasing photoelectrode thickness. Nevertheless, it was discovered that the current density reduced when the Cu_2O photoelectrode film thickness was increased to 1.5μm, i.e., FC4 ~3.08mA/cm^2. The authors reported the photocurrent density of FC3ZG and FC3Z, which were ~ 4.94mA/cm^2 and 4.51mA/cm^2, respectively, at 0V vs. RHE. Compared to the FC3 and FC3Z photoelectrodes, the FC3ZG hybrid photoelectrode demonstrated a greater photocurrent density and improved stability. Overall, the results presented by the authors demonstrate the effectiveness of the synthesized FCZG hybrid photoelectrode in improving PEC performance for water splitting [45].

3. Conclusions

As a green and sustainable energy source, producing green hydrogen by water splitting has attracted a lot of attention. The use of renewable resources is essential for the generation of green hydrogen; however, the present difficulty is addressing the scalability issue. To increase the efficiency of hydrogen production, scientists are investigating a variety of nanocomposites as electrodes or photoelectrode in electrochemical, photochemical, and photoelectrochemical processes. This review paper discusses the electrochemical and photoelectrochemical properties of different rGO and ZnO/rGO nanocomposite-based electrodes and their effectiveness in water-splitting. The photoelectrochemical (PEC) and electrochemical activity of photoelectrodes and electrodes, respectively, for water splitting can be improved by combining reduced graphene oxide (rGO) with metal oxide nanocomposites such as Cu_2O/ZnO, Fe_3O_4-ZnO, $ZnIn_2S_4$, and Ni/NiO-TiO_2. Improved interfacial electron transfer occurs at the electrode/electrolyte interface by adding rGO to metal oxide nanocomposites, which upsurges the interfacial contact area and improves electronic interaction. The introduction of Cu_2O to the ZnO/RGO nanocomposites resulted in the highest photocurrent density, indicating the synergistic effect between rGO, ZnO, and Cu_2O that improves the transport of electrons and reduces the electron-hole recombination rate.

Moreover, at a particular thickness of Cu_2O/ZnO/rGO, photoelectrode showed a promising result of 4.94mA/cm^2 at 0V vs.The RHE for PEC water splitting, which was the highest among the literature reviewed. For electrochemical water splitting, the synthesis of Ni/NiO-TiO_2/rGO electrode using the PECVD method showed the best results as lowest onset potential and tafel slope value of 30mV and 40mV/decade, respectively, and showed longer stability among the literature reviewed. These studies show the potential of rGO-based nanocomposites as effective electrodes for efficient water splitting, which can aid in producing renewable energy sources. To create a more environmentally friendly and sustainable energy scenario, further research is required to investigate more effective electrodes and boost hydrogen production efficiency.

Funding

This research received no external funding.

Acknowledgments

Presented in 4th International Conference on “Recent Advances in Fundamental and Applied Sciences” (RAFAS-2023)” on March 24-25, 2023, Organized by the School of Chemical Engineering and Physical Sciences, Lovely Professional University, Punjab, India.

Conflicts of Interest

The authors declare no conflict of interest.

References

1. Gupta, A.; Likozar, B.; Jana, R.; Chanu, W.C.; Singh, M.K. A review of hydrogen production processes by photocatalytic water splitting – From atomistic catalysis design to optimal reactor engineering. *Int. J. Hydrog. Energy* **2022**, *47*, 33282-33307, https://doi.org/10.1016/j.ijhydene.2022.07.210.
2. Li, X.; Zhao, L.; Yu, J.; Liu, X.; Zhang, X.; Liu, H.; Zhou, W. Water Splitting: From Electrode to Green Energy System. *Nano-Micro Lett.* **2020**, *12*, 131, https://doi.org/10.1007/s40820-020-00469-3.
3. Kotowicz, J.; Uchman, W.; Jurczyk, M.; Sekret, R. Evaluation of the potential for distributed generation of green hydrogen using metal-hydride storage methods. *Appl. Energy* **2023**, *344*, 121269, https://doi.org/10.1016/j.apenergy.2023.121269.
4. Mamur, H.; Dilmaç, Ö.F.; Begum, J.; Bhuiyan, M.R.A. Thermoelectric generators act as renewable energy sources. *Clean. Mater.* **2021**, *2*, 100030, https://doi.org/10.1016/j.clema.2021.100030.
5. Li, J.; Chen, J.; Guo, H. Triboelectric Nanogenerators for Harvesting Wind Energy: Recent Advances and Future Perspectives. *Energies* **2021**, *14*, 6949, https://doi.org/10.3390/en14216949.
6. Jiang, T.; Yao, Y.; Xu, L.; Zhang, L.; Xiao, T.; Wang, Z.L. Spring-assisted triboelectric nanogenerator for efficiently harvesting water wave energy. *Nano Energy* **2017**, *31*, 560-567, https://doi.org/10.1016/j.nanoen.2016.12.004.
7. Hassan, Q.; Abdulateef, A.M.; Hafedh, S.A.; Al-samari, A.; Abdulateef, J.; Sameen, A.Z.; Salman, H.M.; Al-Jiboory, A.K.; Wieteska, S.; Jaszczur, M. Renewable energy-to-green hydrogen: A review of main resources routes, processes and evaluation. *Int. J. Hydrog. Energy* **2023**, *48*, 17383-17408, https://doi.org/10.1016/j.ijhydene.2023.01.175.
8. Du, J.; Xiang, D.; Zhou, K.; Wang, L.; Yu, J.; Xia, H.; Zhao, L.; Liu, H.; Zhou, W. Electrochemical hydrogen production coupled with oxygen evolution, organic synthesis, and waste reforming. *Nano Energy* **2022**, *104*, 107875, https://doi.org/10.1016/j.nanoen.2022.107875.
9. Harshapriya, P.; Basandrai, D.; Kaur, P. Structural and optical properties of Yttrium-Silver doped ZnO nanoparticle. *Mater. Today Proc.* **2023**, https://doi.org/10.1016/j.matpr.2023.01.235.
10. Harshapriya, P.; Kaur, P.; Basandrai, D. Influence of La-Ag substitution on structural, magnetic, optical, and microwave absorption properties of $BiFeO_3$ multiferroics. *Chin. J. Phys.* **2023**, *84*, 119-131, https://doi.org/10.1016/j.cjph.2023.03.021.
11. Harshapriya, P.; Basandrai, D.; Kaur, P. Structural, magnetic, microwave absorption and electromagnetic properties of Y-Ag-doped bismuth ferrite nanoparticles for commercial applications. *Appl. Phys. A* **2023**, *129*, 316, https://doi.org/10.1007/s00339-023-06535-y.
12. Wei, C.; Rao, R.R.; Peng, J.; Huang, B.; Stephens, I.E.L.; Risch, M.; Xu, Z.J.; Shao-Horn, Y. Recommended Practices and Benchmark Activity for Hydrogen and Oxygen Electrocatalysis in Water Splitting and Fuel Cells. *Adv. Mater.* **2019**, *31*, 1806296, https://doi.org/10.1002/adma.201806296.
13. Bard, A.J.; Faulkner, L.R. Electrochemical Methods: Fundamentals and Applications, 2nd Edition, John Wiley& Sons, **2001**, 482.
14. Sun, H.; Xu, X.; Kim, H.; Jung, W.; Zhou, W.; Shao, Z. Electrochemical Water Splitting: Bridging the Gaps Between Fundamental Research and Industrial Applications. *Energy Environ. Mater.* **2023**, *6*, e12441, https://doi.org/10.1002/eem2.12441.
15. Linsebigler, A.L.; Lu, G.; Yates Jr., J.T. Photocatalysis on TiO_2 Surfaces: Principles, Mechanisms, and Selected Results. *Chem. Rev.* **1995**, *95*, 735-758, https://doi.org/10.1021/cr00035a013.
16. Walter, M.G.; Warren, E.L.; McKone, J.R.; Boettcher, S.W.; Mi, Q.; Santori, E.A.; Lewis, N.S. Solar Water Splitting Cells. *Chem. Rev.* **2010**, *110*, 6446-6473, https://doi.org/10.1021/cr1002326.
17. Kumar, M.; Meena, B.; Subramanyam, P.; Suryakala, D.; Subrahmanyam, C. Recent trends in photoelectrochemical water splitting: the role of co-catalysts. *NPG Asia Mater.* **2022**, *14*, 88, https://doi.org/10.1038/s41427-022-00436-x.
18. Ni, M.; Leung, M.K.H.; Leung, D.Y.A; Sumathy, K. A review and recent developments in photocatalytic water-splitting using TiO_2 for hydrogen production. *Renew. Sustain. Energy Rev.* **2007**, *11*, 401-425, https://doi.org/10.1016/j.rser.2005.01.009.
19. Mikaeili, F.; Gilmore, T.; Gouma, P.-I. Photochemical Water Splitting via Transition Metal Oxides. *Catalysts* **2022**, *12*, 1303, https://doi.org/10.3390/catal12111303.

20. Sawant, J.P.; Pathan, H.M.; Kale, R.B. Photoelectrochemical Properties of Spray Deposited Cu_2ZnSnS_4 Photoelectrode: Enhancement in Photoconversion Efficiency with Film Thickness. *ES Energy Environ.* **2020**, *10*, 73-79, http://dx.doi.org/10.30919/esee8c933.
21. Chen, Z.; Dinh, H.N.; Miller, E. Photoelectrochemical Water Splitting, Springer, New York, **2013**, Volume 344, 6-15, https://doi.org/10.1007/978-1-4614-8298-7.
22. Li, J.; Qiu, Y.; Wei, Z.; Lin, Q.; Zhang, Q.; Yan, K.; Chen, H.; Xiao, S.; Fan, Z.; Yang, S. A three-dimensional hexagonal fluorine-doped tin oxide nanocone array: a superior light harvesting electrode for high performance photoelectrochemical water splitting. *Energy Environ. Sci.* **2014**, *7*, 3651-3658, http://doi.org/10.1039/C4EE01581A.
23. Zhao, Y.; Niu, Z.; Zhao, J.; Xue, L.; Fu, X.; Long, J. Recent Advancements in Photoelectrochemical Water Splitting for Hydrogen Production. *Electrochem. Energy Rev.* **2023**, *6*, 14, https://doi.org/10.1007/s41918-022-00153-7.
24. Wang, J.; Yang, W.; Liu, J. CoP_2 nanoparticles on reduced graphene oxide sheets as a super-efficient bifunctional electrocatalyst for full water splitting. *J. Mater. Chem.* A **2016**, 4, 4686-4690, http://dx.doi.org/10.1039/C6TA00596A.
25. Souza, V.H.R.; Husmann, S.; Neiva, E.G.C.; Lisboa, F.S.; Lopes, L.C.; Salvatierra, R.V.; Zarbin, A.J.G. Flexible, Transparent and Thin Films of Carbon Nanomaterials as Electrodes for Electrochemical Applications. *Electrochim. Acta* **2016**, *197*, 200–209, https://doi.org/10.1016/j.electacta.2015.08.077.
26. Salvatierra, R.V.; Oliveira, M.M.; Zarbin, A.J.G. One-Pot Synthesis and Processing of Transparent, Conducting, and Freestanding Carbon Nanotubes/Polyaniline Composite Films. *Chem. Mater.* **2010**, *22*, 5222–5234, https://doi.org/10.1021/cm1012153.
27. Neiva, E.G.C.; Oliveira, M.M.; Bergamini, M.F.; Marcolino Jr., L.H.; Zarbin, A.J.G. One material, multiple functions: graphene/$Ni(OH)_2$ thin films applied in batteries electrochromism and sensors. *Sci. Rep.* **2016**, *6*, 33806, https://doi.org/10.1038/srep33806.
28. Romeiro, F.C.; Rodrigues, M.A.; Silva, L.A.J.; Catto, A.C.; da Silva, L.F.; Longo, E.; Nossol, E.; Lima, R.C. rGO-ZnO nanocomposites for high electrocatalytic effect on water oxidation obtained by microwave-hydrothermal method. *Appl. Surf. Sci.* **2017**, *423*, 743–751, https://doi.org/10.1016/j.apsusc.2017.06.221.
29. Narwade, S.S.; Mali, S.M.; Digraskar, R.V.; Sapner, V.S.; Sathe, B.R. Ni/NiO@rGO as an efficient bifunctional electrocatalyst for enhanced overall water splitting reactions. *Int. J. Hydrog. Energy* **2019**, *44*, 27001-27009, https://doi.org/10.1016/j.ijhydene.2019.08.147.
30. Nada, A.A.; Bekheet, M.F.; Roualdes, S.; Gurlo, A.; Ayral, A. Functionalization of MCM-41 with titanium oxynitride deposited via PECVD for enhanced removal of methylene blue. *J. Mol. Liq.* **2019**, *274*, 505-515, https://doi.org/10.1016/j.molliq.2018.10.154.
31. Nada, A.A.; Nasr, M.; Viter, R.; Miele, P.; Roualdes, S.; Bechelany, M. Mesoporous $ZnFe_2O_4$@TiO_2 Nanofibers Prepared by Electrospinning Coupled to PECVD as Highly Performing Photocatalytic Materials. *J. Phys. Chem. C* **2017**, *121*, 24669-24677, https://doi.org/10.1021/acs.jpcc.7b08567.
32. El-Maghrabi, H.H.; Nada, A.A.; Roualdes, S.; Bekheet, M.F. Design of Ni/NiO-TiO_2/rGO nanocomposites on carbon cloth conductors via PECVD for electrocatalytic water splitting. *Int. J. Hydrog. Energy* **2020**, *45*, 32000-32011, https://doi.org/10.1016/j.ijhydene.2020.08.259.
33. Pan, Z.-Y.; Tang, Z.; Zhan, Y.-Z.; Sun, D. Three-dimensional porous $CoNiO_2$@reduced graphene oxide nanosheet arrays/nickel foam as a highly efficient bifunctional electrocatalyst for overall water splitting. *Tungsten* **2020**, *2*, 390–402, https://doi.org/10.1007/s42864-020-00065-3.
34. Cao, L.; Li, Z.; Su, K.; Zhang, M.; Cheng, B. Rational design of hollow oxygen deficiency-enriched $NiFe_2O_4$@N/rGO as bifunctional electrocatalysts for overall water splitting. *J. Energy Chem.* **2021**, *54*, 595-603, https://doi.org/10.1016/j.jechem.2020.06.053.
35. Arif, M.; Yasin, G.; Shakeel, M.; Mushtaq, M.A.; Ye, W.; Fang, X.; Ji, S.; Yan, D. Highly active sites of NiVB nanoparticles dispersed onto graphene nanosheets towards efficient and pH-universal overall water splitting. *J. Energy Chem.* **2021**, *58*, 237-246, https://doi.org/10.1016/j.jechem.2020.10.014.
36. Li, H.; Chen, L.; Jin, P.; Li, Y.; Pang, J.; Hou, J.; Peng, S.; Wang, G.; Shi, Y. $NiCo_2S_4$ microspheres grown on N, S co-doped reduced graphene oxide as an efficient bifunctional electrocatalyst for overall water splitting in alkaline and neutral pH. *Nano Res.* **2022**, *15*, 950-958, https://doi.org/10.1007/s12274-021-3580-z.
37. Kareem, A.; Maiyalagan, T. Influence of carbonaceous materials supported nanostructured nickel phosphide as an electrocatalyst for the hydrogen evolution reaction. *Ceram. Int.* **2022**, *48*, 29087-29092, https://doi.org/10.1016/j.ceramint.2022.05.026.

38. Yusoff, N.; Kumar, S.V.; Pandikumar, A.; Huang, N.M.; Marlinda, A.R.; An'amt, M.N. Core-shell Fe_3O_4-ZnO nanoparticles decorated on reduced graphene oxide for enhanced photoelectrochemical water splitting. *Ceram. Int.* **2015**, *41*, 5117-5128, https://doi.org/10.1016/j.ceramint.2014.12.084.
39. Bai, Z.; Yan, X.; Kang, Z.; Hu, Y.; Zhang, X.; Zhang, Y. Photoelectrochemical performance enhancement of ZnO photoanodes from $ZnIn_2S_4$ nanosheets coating. *Nano Energy* **2015**, *14*, 392-400, https://doi.org/10.1016/j.nanoen.2014.09.005.
40. Khan, I.; Ibrahim, A.A.M.; Sohail, M.; Qurashi, A. Sonochemical assisted synthesis of RGO/ZnO nanowire arrays for photoelectrochemical water splitting. *Ultrason. Sonochem.* **2017**, *37*, 669-675, https://doi.org/10.1016/j.ultsonch.2017.02.029.
41. Ghorbani, M.; Abdizadeh, H.; Taheri, M.; Golobostanfard, M.R. Enhanced photoelectrochemical water splitting in hierarchical porous ZnO/Reduced graphene oxide nanocomposite synthesized by sol-gel method. *Int. J. Hydrog. Energy* **2018**, *43*, 7754-7763, https://doi.org/10.1016/j.ijhydene.2018.03.052.
42. Zhang, H.; Tian, W.; Li, Y.; Sun, H.; Tadéa, M.O.; Wang, S. A comparative study of metal (Ni, Co, or Mn)-borate catalysts and their photodeposition on rGO/ZnO nanoarrays for photoelectrochemical water splitting. *J. Mater. Chem. A* **2018**, *6*, 24149-24156, https://doi.org/10.1039/C8TA06921B.
43. Wang, J.; Wang, G.; Jiang, J.; Wan, Z.; Su, Y.; Tang, H. Insight into charge carrier separation and solar-light utilization: rGO decorated 3D ZnO hollow microspheres for enhanced photocatalytic hydrogen evolution. *J. Colloid Interface Sci.* **2020**, *564*, 322-332, https://doi.org/10.1016/j.jcis.2019.12.111.
44. Murali, A.; Sarswat, P.K.; Free, M.L. Minimizing electron-hole pair recombination through band-gap engineering in novel ZnO-CeO_2-rGO ternary nanocomposite for photoelectrochemical and photocatalytic applications. *Environ. Sci. Pollut. Res.* **2020**, *27*, 25042–25056 https://doi.org/10.1007/s11356-020-08990-z.
45. Shanmugasundaram, A.; Johar, M.A.; Boppella, R.; Kim, D.-S.; Jeong, Y.-J.; Kim, J.Y.; Hassan, M.A.; Ryu, S.-W.; Lee, D.W. Stabilizing nanocrystalline Cu_2O with ZnO/rGO: Engineered photoelectrodes enables efficient water splitting. *Ceram. Int.* **2021**, *47*, 7558-7570, https://doi.org/10.1016/j.ceramint.2020.11.094.